



Temperature dependence of gypsum dissolution rates

Qingxu Jin^{a,b,1}, LaKeshia N. Perry^a, Jeffrey W. Bullard^{a,1,*}

^a Materials and Structural Systems Division, Engineering Laboratory, National Institute of Standards and Technology, Gaithersburg, MD 20899, USA

^b School of Civil and Environmental Engineering, Georgia Institute of Technology, Atlanta, GA 30332, USA



ARTICLE INFO

Keywords:

Gypsum
Dissolution
Kinetics
Activation energy
Surface area

ABSTRACT

The reaction kinetics of gypsum dissolution are important for establishing an optimum gypsum content in portland cement. In this paper, the temperature dependence of dissolution rates was measured by tracking changes in solution composition and surface area with time. The rate coefficient increases with temperature and the specific surface area decreases with ongoing dissolution. The dissolution rate depends on the solution's saturation index to an exponent of approximately 1.5. The apparent activation enthalpy is approximately 34 kJ mol⁻¹, independent of saturation index and surface area, suggesting that dissolution is controlled by surface reaction rather than mass transport. The activation enthalpy is interpreted as the energy required to cooperatively break all the ionic bonds at occupied kink sites of the gypsum-water interface. Activation enthalpies similar in magnitude have been reported for other calcium salts, which may indicate that all of these processes involve breaking ionic calcium-oxygen bonds of similar strengths.

1. Introduction

Cement hydration comprises numerous chemical reactions and mass transport phenomena, including the dissolution of solid cementitious components, diffusion or advection of ions in solution, and the precipitation of cementitious hydrates from a supersaturated solution. The thermodynamic properties of many of the more prevalent phases in portland cement, portland limestone cement, calcium aluminate and sulfoaluminate cements, and blended cements have been measured [1-5]. However, far fewer attempts have been made to establish the kinetics of the cement hydration reactions. Understanding the reaction kinetics of the components in portland cement, especially the dissolution kinetics [6], will likely be increasingly important in the future for optimizing the design of cement-based materials. This paper takes another step in that direction by clarifying the temperature dependence of gypsum dissolution rates.

Gypsum powder characteristics, as well as its intrinsic dissolution rate, are important for regulating the hydration reactions of tricalcium aluminate in binders containing portland cement or certain Class C fly ashes [7-9]. Previous efforts have been made to understand gypsum dissolution kinetics in terms of its dependence on particle size or surface area [10-13] and its dependence on relative saturation as a measure of thermodynamic driving force [13,14]. The temperature dependence, however, has not been widely reported, even though the temperature

can vary widely among construction jobs [15,16]. The current paper measures the temperature dependence of gypsum dissolution rates, taking into account both the evolution in its surface area and the degree of saturation of the solution.

1.1. Background on gypsum dissolution

Most measurements of gypsum powder dissolution rates are made by monitoring the change in solution composition of a stirred powder suspension [10,13], likely because the setup is simple and can mimic the real situation of gypsum-water interactions during cement hydration. The rotating disc method has also been used to measure gypsum's dissolution rate and its temperature dependence [11,17,18]. The latter method can distinguish diffusion controlled kinetics from reaction control, but it does not accurately mimic the real situation of gypsum dissolution because it disregards the effects of particle size and surface area on dissolution rate.

Gypsum dissolution has also been interrogated using single crystals instead of powders. Atomic (or scanning) force microscopy [19-25], vertical scanning interferometry [26], and digital holographic microscopy [27] all have been used for that purpose. Those methods are able to capture the change of surface topography and the effects of features such as etch pits on gypsum dissolution. However, the observed rates are between 10 and 100 times less than those measured on powders in a

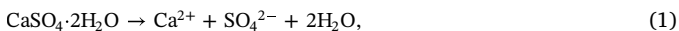
* Corresponding author.

E-mail addresses: billjin@gatech.edu (Q. Jin), lakesha.perry@nist.gov (L.N. Perry), jwbullard@tamu.edu (J.W. Bullard).

¹ Current address: Zachry Department of Civil and Environmental Engineering, Texas A&M University, College Station, TX 77843, USA.

stirred suspension [27,28]. Therefore, this study uses powders in a stirred suspension at specified temperatures to determine the temperature dependence of gypsum dissolution rates.

The dissolution of gypsum,



has a standard Gibbs energy change of $\Delta G^\circ = 26.1 \text{ kJ mol}^{-1}$, yielding a solubility product of $K = 2.51 \times 10^{-5}$. The net rate of gypsum dissolution can be described by an equation of the form [13,14,29]

$$J = J_0 \left[1 - \left(\frac{Q}{K} \right)^\alpha \right]^n, \quad (2)$$

where J is the surface normalized rate ($\text{mmol m}^{-2} \text{ s}^{-1}$), J_0 is the surface normalized rate in pure water, Q is the ion activity product, and α and n are empirically-determined exponents. J_0 has the strongest temperature dependence among the terms in Eq. (2) and, by analogy to transition state theory for elementary reactions [30,31], the temperature dependence of J_0 is assumed to have the Arrhenius form,

$$J_0(T) = J_\infty \exp\left(\frac{-\Delta G^*}{RT}\right) \quad (3)$$

where J_∞ is assumed to be constant, ΔG^* is an apparent activation Gibbs energy of dissolution from the reactants to products (Fig. 1), R is the ideal gas constant, and T is the absolute temperature.

2. Materials and methods

2.1. Materials

All experiments were performed with reagent grade calcium sulfate dihydrate (Sigma Aldrich, St. Louis, MO, USA)² with a stated purity exceeding 98 %. Its specific surface area, S_0 , was determined by Brunauer-Emmett-Teller (BET) multipoint N_2 adsorption-desorption isotherms using approximately 1.5 g of the gypsum powder. Measurements of three randomly selected samples yielded $S_0 = (668 \pm 39) \text{ m}^2 \text{ kg}^{-1}$. The particle size distribution (PSD) was also measured in triplicate using laser diffraction in a dilute isopropanol suspension. Fig. 2 shows the differential particle size distribution on both a volume and a number basis. The number-based distribution is unimodal with a sharp peak centered at about $1 \mu\text{m}$. However, laser diffraction is unreliable at particle sizes less than about $1 \mu\text{m}$, so the dry powder was also examined by scanning electron microscopy (SEM). Fig. 3 indicates that the powder does indeed have a multimodal size distribution, and that the surface of larger particles are decorated by much smaller particles. The smaller particles are attracted strongly enough to the larger particles that even aggressive ethanol washing cannot remove them.

2.2. Dissolution experiments

A prescribed mass of $(2.00 \pm 0.01) \text{ g}$ of gypsum powder was added to $(500 \pm 1) \text{ mL}$ of continuously stirred, freshly deionized water ($18.2 \text{ M}\Omega \text{ cm}$). The reported uncertainties are based on the certificates of calibration on the mass balance and volumetric flask, respectively. Prior to adding the powder, the container was immersed and thermally equilibrated in a water bath that maintained a fixed temperature to within $0.1 \text{ }^\circ\text{C}$. Continuous stirring was maintained by a polypropylene swing-out paddle propeller (Cole-Parmer, Vernon Hills, IL, USA).

The suspension was periodically sampled by withdrawing a $(5.0 \pm 0.1) \text{ mL}$ aliquot of the solution and passing it through a $0.2 \mu\text{m}$

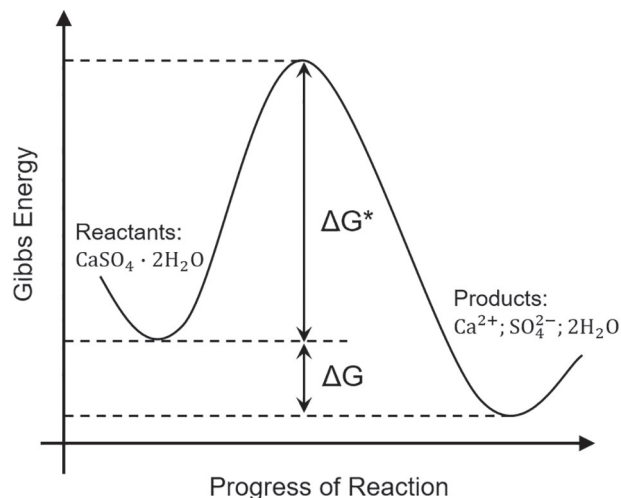


Fig. 1. The Gibbs activation energy (ΔG^*) for gypsum dissolution is the difference between the highest energy position (peak position) and the energy state of reactants. ΔG is the Gibbs energy of the reaction.

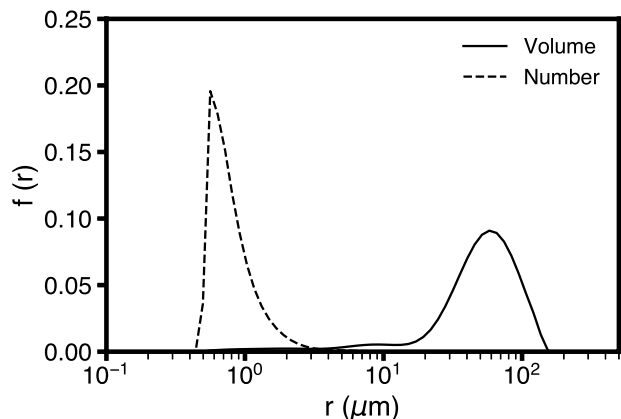


Fig. 2. Differential particle size distribution, on both a volume and a number basis, of the initial gypsum powder.

filter; the acts of withdrawing and filtering took $(5 \pm 1) \text{ s}$. The total interval between successive samplings was $(10 \pm 1) \text{ s}$, and the sampling procedure continued for 120 s . The reported uncertainties in aliquot volume and withdrawal times are based on the standard deviation of three replicate measurements.

Dissolved components in each aliquot were stabilized with $100 \mu\text{L}$ of dilute nitric acid (5 % by mass). The solution was then sealed in a plastic centrifuge tube and refrigerated at $\leq 3 \text{ }^\circ\text{C}$ while awaiting measurements of composition. The elemental concentrations of calcium and sulfur in the solution were measured in triplicate by inductively coupled plasma optical emission spectrometry (ICP-OES), using yttrium as an internal standard according to a previously described procedure [13].

The influence of stirring rate on dissolution was first checked by measuring the change in solution composition with time, using a method described by Tang et al. [13]. The concentration profiles were approximately independent of stirring rate when the stirring rate was at least 250 rpm (0.44 rad s^{-1}), signifying that the dissolution rate is controlled by a surface process instead of mass transport through the solution. All the subsequent experiments were performed at a stirring rate of 250 rpm . The temperature dependence of the dissolution rate was investigated by performing the dissolution experiments just described at $10 \text{ }^\circ\text{C}$, $15 \text{ }^\circ\text{C}$, $20 \text{ }^\circ\text{C}$, and $25 \text{ }^\circ\text{C}$. The temperature range was selected to ensure lower dissolution rates that could be measured more accurately.

²Certain commercial equipment, instruments, or materials are identified in this paper to foster understanding. Such identification does not imply recommendation or endorsement by the National Institute of Standards and Technology, nor does it imply that the materials or equipment identified are necessarily the best available for the purpose.

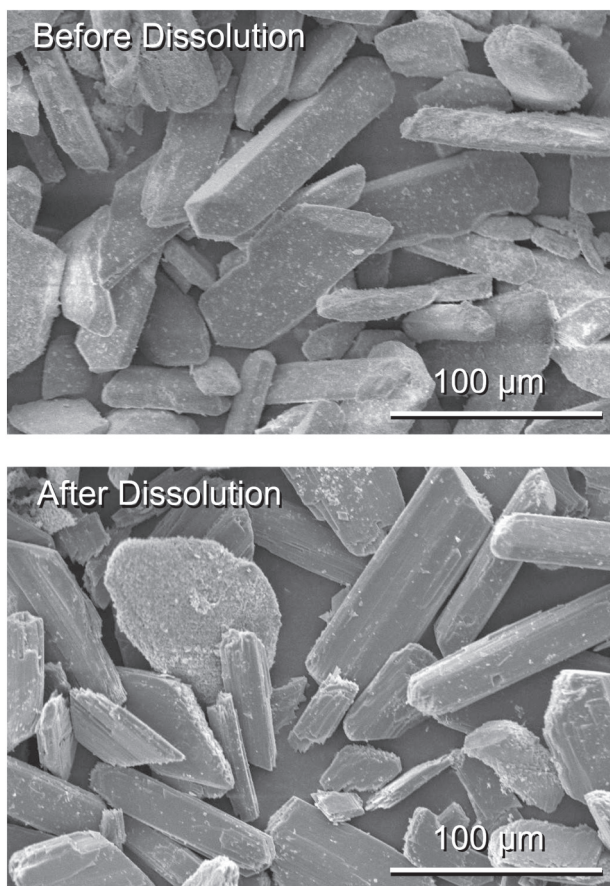


Fig. 3. SEM analysis for gypsum powder particles before and after dissolution.

2.3. Calculations of dissolution rate

The instantaneous surface normalized dissolution rate is

$$J = -\frac{1}{A} \frac{dN}{dt} = \frac{V}{mS} \frac{dc}{dt} \quad (4)$$

where A is the total powder surface area, N is the number of moles of gypsum powder, V is the solvent volume, m and S are the powder mass and specific surface area, respectively, and c is the solution concentration. The relative saturations of the solution, Q/K in Eq. (2), were obtained from the measured elemental concentrations of Ca and S using the Gibbs Energy Minimization program (GEM-Selektor) [32], with the supplemental thermodynamic database `cemdata18` [33].

The mass change at each sampling time, $\Delta m(t)$, can be expressed as a function of the measured concentration change,

$$\Delta m(t) = -VM[c(t) - c_0] \quad (5)$$

where M is the molar mass of gypsum, $c(t)$ is the solution concentration at sampling time t , and c_0 is the initial solution concentration. A negative sign is used in Eq. (5) because $\Delta m(t)$ is a negative value, representing a mass loss in dissolution.

Changes in specific surface area during dissolution were estimated by partially dissolving multiple samples of gypsum powder in deionized water to obtain varying dissolved fractions of initial powder mass. The residual powder was filtered with cold deionized water ($\leq 3^\circ\text{C}$), rapidly dried to minimize the possibility of precipitation, and then subjected to BET and SEM analysis to characterize the specific surface area and morphology, respectively. SEM observations confirmed that little or no precipitation happened during the filtering and drying procedure (Fig. 3). These measurements were performed separately because BET analysis requires significantly more powder mass than that used in the

dissolution experiments (Section 2.1). The dependence of specific surface area on mass change was modeled from these data by nonlinear regression and was taken into account in calculations of the surface normalized dissolution rate, as discussed further in Section 3.1.

2.4. Calculations of temperature dependence

Eq. (3) can be rewritten as

$$\begin{aligned} \ln J_0(T) &= \ln J_\infty - \frac{\Delta G^*}{RT} \\ &= \ln J_\infty - \frac{\Delta H^* - T\Delta S^*}{RT} \\ &= \left(\ln J_\infty + \frac{\Delta S^*}{R} \right) - \frac{\Delta H^*}{RT} \end{aligned} \quad (6)$$

where ΔH^* and ΔS^* are the apparent activation enthalpy and activation entropy, respectively. The temperature dependence of gypsum dissolution rates is characterized here by the value of ΔH^* , which is obtained from the slope of a plot of $\ln J$ against $1/T$.

3. Results

3.1. Surface area changes and rate equation

Fig. 4 plots the specific surface area, normalized by its initial value, as a function of the fractional change in mass, $(-\Delta m/m_0)$. The sharp decrease in S/S_0 from its initial value of unity during the first 10 % of mass loss (Fig. 4) is likely caused by the annihilation of the many small particles evident in Fig. 3. These small particles make a large contribution to the surface area but much less contribution to the total solid volume. The remaining analysis of dissolution rates will therefore consider only the regime after the first 10 % of mass loss because we were unable to accurately capture the rapid changes in surface area during that initial time. Therefore, discarding the implicit point at $S/S_0 = 1$, the specific surface area is modeled as a linear function of mass loss

$$\frac{S}{S_0} = a + b \frac{\Delta m(t)}{m_0}. \quad (7)$$

The parameters $\{a, b\}$ are obtained by linear regression as $\{0.54 \pm 0.03, 0.35 \pm 0.16\}$, with the quoted uncertainties representing the 95 % confidence intervals of the parameter estimates. The fit is shown as a solid line in Fig. 4.

Two other commonly assumed models of specific surface area are

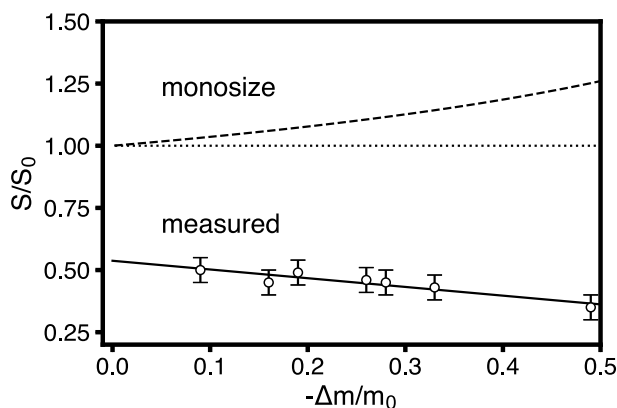


Fig. 4. Normalized specific surface area as a function of the fraction of powder mass dissolved in deionized water. The solid line is the mathematical model in the form of Eq. (7), which is obtained by linear regression on the experimental data. The dashed line represents particles shrinking uniformly at a constant shape. The dotted line represents the specific surface area remaining constant during the particle dissolution.

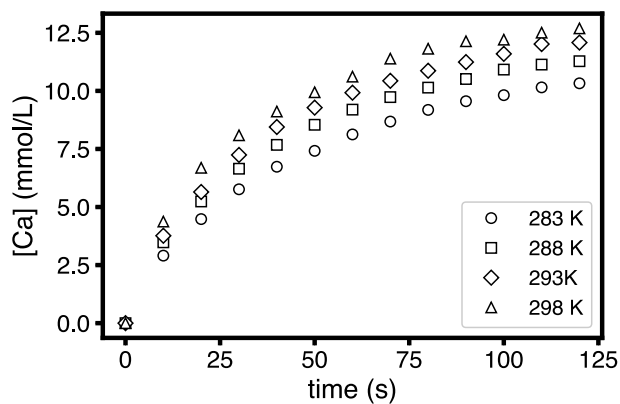


Fig. 5. Measured concentration profiles at different temperatures. The coefficient of variation for time and concentration measurements, estimated by three replicate measurements, is less than 10% and 1%, respectively. Corresponding error bars are about the size of the symbols and are omitted for clarity.

also plotted for comparison in Fig. 4. The dashed line represents monosized particles shrinking uniformly at a constant shape, in which case S/S_0 varies with the change of the mass as $(m/m_0)^{-1/3}$ regardless of the shape. The horizontal dotted line assumes that the particles retain a constant specific surface area as they dissolve. These commonly assumed models are shown in the plot merely to draw attention to the errors that would arise if used to characterize dissolution rate measurements, which in this case become increasingly severe with ongoing dissolution.

The evolution of measured concentration during the dissolution is shown at each temperature in Fig. 5. The concentration increases monotonically with time, with rates that are initially greater with increasing temperature. At each temperature, the rate slows with increasing time as the solution becomes increasingly saturated.

The concentration data in Fig. 5 can be used to infer the average dissolution rate during any time interval [13],

$$\begin{aligned} \bar{J} &\equiv \frac{1}{t} \int_0^t \frac{V}{mS(\tau)} \frac{dc}{d\tau} d\tau \\ &= \frac{1}{S_0 M t} \int_0^{VM(c_f - c_0)/m_0} \frac{dx}{(1-x)(a-bx)} \end{aligned} \quad (8)$$

where \bar{J} is the average surface normalized rate over a time interval, S_0 is the specific surface area at the beginning of that time interval, M is the molar mass of gypsum ($0.172 \text{ kg mol}^{-1}$), t is the length of the time interval, V is the volume of solution remaining in the reactor at the beginning of the given time interval, c_0 and c_f are the dissolved concentrations at the start and end of the time interval, respectively, and m_0 is the mass of powder in the reactor at the beginning of the time interval. Eq. (7) is substituted to obtain the final form, with $\{a, b\}$ being the regression parameters previously determined. The measurement uncertainties in concentrations, surface area, and time interval were propagated to an inferred uncertainty in average rate by assuming that each of the uncertain components are normally distributed about their mean. For each time interval, Eq. (8) was evaluated 1000 times by Gaussian quadrature, each time randomly sampling values of the uncertain components from their assumed distributions. The average rates and their uncertainties are reported as the means and sample standard deviations of these 1000 samples.

3.2. Rate dependence on Q/K and temperature

The dissolution rates for each temperature were calculated using the procedure in the previous section and plotted against Q/K , as shown in Fig. 6. The rates can be modeled using Eq. (2), and nonlinear regression of the data to that equation at each temperature gives the optimum values of J_0 and n as catalogued in Table 1. As in a previous study of

gypsum dissolution [13], the lowest standard errors of regression are obtained with $\alpha = 1$ in Eq. (2).

The rate coefficient J_0 increases with temperature as expected, with the rates at 25°C being about double the rates at 10°C . The results at 25°C are consistent with those of previous studies at room temperature [10]. The exponent n in Eq. (2) is about 1.5 over the range of temperatures examined (Table 1). The temperature insensitivity of the exponent suggests that the surface reaction is not qualitatively affected by temperature.

Plots of $\ln J$ versus $1/T$ at four different saturation levels are shown in Fig. 7. The data appear to be nearly linear at each saturation; any slight nonlinearity that might be present is well within the experimental uncertainty indicated by the error bars in the plot. The relationship between average dissolution rate and Q/K , represented by the fitted curve in Fig. 6, was used to interpolate the ΔH^* at exact Q/K values using Eq. (6). Table 2 summarizes the ΔH^* value obtained at each Q/K from the slopes obtained by linear regression.

A slight increase in ΔH^* with Q/K may be indicated by the data, but the magnitude falls within the margin of uncertainty in the slopes. Consequently, the activation enthalpy is assumed to be approximately constant within this intermediate range of Q/K , with a value of $\Delta H^* \approx (34 \pm 4) \text{ kJ mol}^{-1}$.

4. Discussion

The ideal metric for surface normalization of rates of crystal dissolution should be the number density of the sites that are associated with the greatest local dissolution rates. Numerous studies have shown that these sites contribute almost all of the macroscopic dissolution flux while the greater majority of the surface remains relatively inert [27,34–39]. These are primarily kink sites, which are those surface sites at which an atom has half the number of chemical bonds as the equivalent site in the bulk. The topographic surface features that are often observed to have the greatest dissolution rates, such as steps, corners, and etch pits, are locations where the number of kink sites per unit area is relatively high [25,27,34–40]. However, the absence of a straightforward technique for characterizing the number density of kinks means that some other measure of surface area must be used instead. Among the various available methods, those that use molecular adsorption, such as BET adsorption-desorption isotherms, are able to detect at least the relevant topographic features—steps, etch pits—if not the actual number density of kink sites. Geometric measurements, such as average particle size coupled with an assumed shape [10,18], are not sensitive to these kinds of features. Therefore, one might expect BET specific surface areas to at least be more closely related than geometric estimates to the number density of reactive surface sites.

This study and a recent one by Tang et al. [13], both performed on gypsum powders, are the only two of which we know that attempted to experimentally monitor changes in the powder's specific surface area, S , as it dissolves. It is experimentally quite challenging to measure surface area changes like this, but having some notion of how S evolves during dissolution is important because instantaneous rates depend on instantaneous surface area, not on the initial surface area. Unfortunately, those two studies report significantly different changes in S with ongoing dissolution, even for reagent grade powder obtained from the same manufacturer. The earlier study reported that S increases steadily with mass loss (Fig. 4a of Reference [13]), while the current study observed a rapid decrease in S initially, followed by a continuing but slower decrease thereafter (Fig. 4). We can think of two possible reasons for these different outcomes. First, the powder used in this study had a high initial concentration of very small particles (Fig. 3) compared to the powder used by Tang (Fig. 1 of Reference [13]). The rapid annihilation of those small particles in this study should decrease S substantially and likely overwhelms any increases caused by shrinkage or roughening of the remaining particles. This same occurrence of many extremely small particles is often observed for crushed or ground

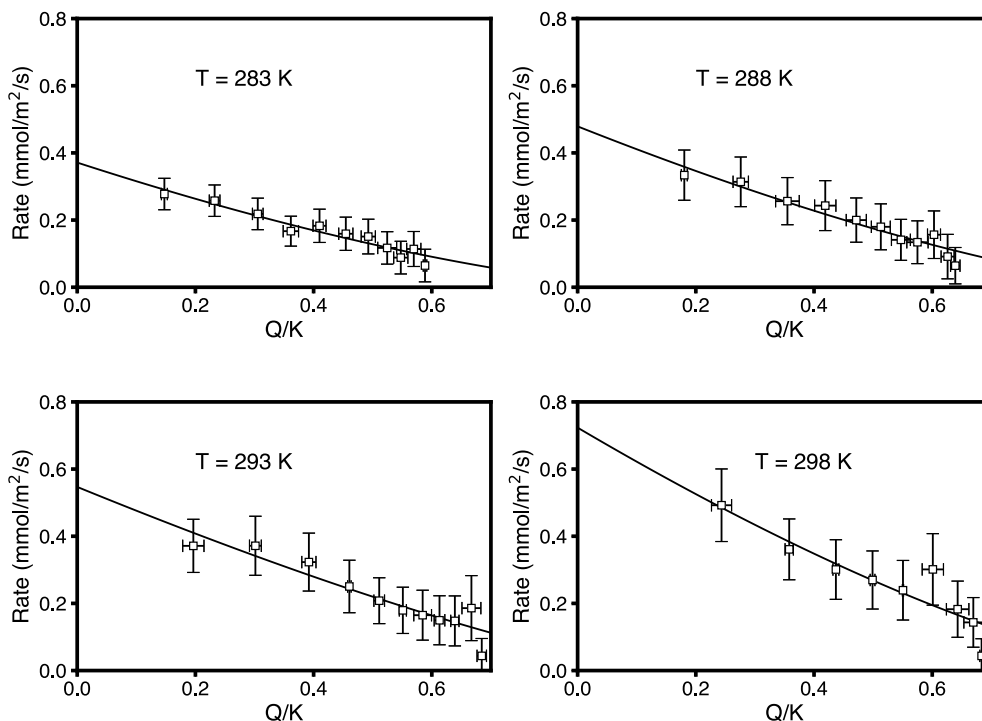


Fig. 6. The average dissolution rates for temperatures of 288 K–298 K as a function of average Q/K . The uncertainty is given in terms of 95% confidence intervals based on propagation of component uncertainties, randomly sampling from the assumed normal distributions of each uncertain component 1000 times.

Table 1

Nonlinear regression of the parameters in Eq. (2) with $\alpha = 1$ enforced. The inferred rate at zero saturation ($Q/K = 0$), J_0 , is reported together with the exponent n . Uncertainties represent 95% confidence intervals of the parameter estimates.

T (K)	J_0 ($\text{mmol m}^{-2} \text{s}^{-1}$)	n
283	0.37 ± 0.06	1.54 ± 0.32
288	0.48 ± 0.08	1.46 ± 0.32
293	0.54 ± 0.13	1.29 ± 0.40
298	0.71 ± 0.20	1.41 ± 0.45

Table 2

Linear regression estimates of the parameters in Eq. (6). The apparent activation enthalpy (ΔH^*) is obtained from the slope of $\Delta H^*/(1000R)$, where R is the ideal gas constant ($8.314 \text{ J mol}^{-1} \text{ K}^{-1}$). Therefore, multiplying the slope by R gives ΔH^* in units of kJ mol^{-1} . The first column of ΔH^* is based on the empirically determined model, Eq. (7). The second and third columns of ΔH^* are based on the assumptions of uniform shrinking of monosized particles and constant specific surface area (SSA), respectively. Reported uncertainties represent 64% confidence intervals.

Q/K	ΔH^* (kJ mol^{-1})		
	Empirical	Uniform shrinking	Constant SSA
0.3	33.3 ± 3.6	29.1 ± 3.4	29.2 ± 1.9
0.4	33.6 ± 3.9	30.4 ± 3.1	31.1 ± 2.0
0.5	34.8 ± 3.2	32.3 ± 2.6	32.9 ± 2.7
0.6	36.2 ± 3.2	32.9 ± 3.4	34.3 ± 4.4

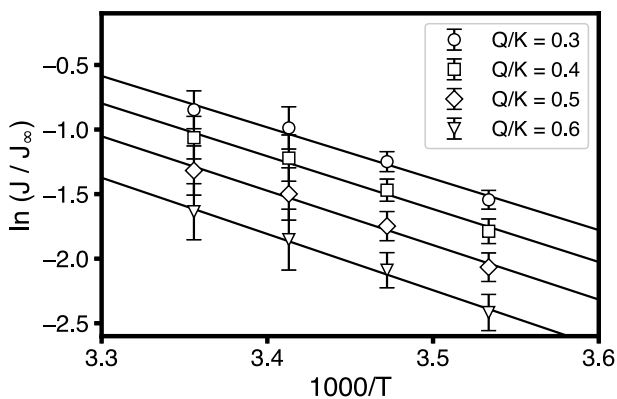


Fig. 7. Dependence of $\ln J$ on $1000/T$ (in Kelvin). The activation enthalpy is approximately constant within this intermediate range of Q/K , with a value of $\Delta H^* \approx 34 \pm 4 \text{ kJ mol}^{-1}$. The uncertainty is obtained from the linear regression estimates of Eq. (6); the error bars represent 64% confidence intervals.

materials, so the surprising evolution in specific surface area observed here may be more common than previously thought. The powder used by Tang, however, was more unusual and did not undergo a rapid disappearance of so many small particles, so the powder's greatest

changes during dissolution are particle shrinkage and roughening, both of which increase S . A second possible reason for the different trends is the different methods used to arrest dissolution at intermediate points. Tang et al. stopped dissolution by adding large volumes of ethanol and rapidly removing the liquid by vacuum filtering [13]. It is now known that calcium sulfate is insoluble in ethanol. In fact, additions of ethanol to a gypsum suspension can cause a milky precipitate of calcium sulfate to form, which could contribute to an erroneously high S if not removed. The procedure used in that study attempted to minimize the influence of this effect by using multiple cycles of ethanol flushing and filtering, which appeared to wash away the milky material with the liquid. In addition, SEM examination of the partially dissolved powders showed no evidence of any residual precipitation (Fig. 5 of Reference [13]). Even so, the current study avoided ethanol and its attendant complications by vacuum filtering with cold deionized water ($\leq 3^\circ\text{C}$).

Regardless of the reasons for the different observed changes in S just discussed, those differences do seem to influence the inferred rate coefficient. J_0 at 25°C was calculated here to be $0.71 \text{ mmol m}^{-2} \text{ s}^{-1}$

(Table 1), which is about three times greater than that reported by Tang et al. at nearly the same temperature of 23 °C [13]. The maximum difference in reported S/S_0 is also about a factor of three between those two studies, which is unlikely to be a coincidence. Despite the attempts in Tang's procedure to remove the influences of precipitation during ethanol flushing, the corresponding differences in J_0 between the two studies implies that precipitation caused at least some artificial inflation of their specific surface areas.

Small particles contribute disproportionately to the powder's specific surface area, but they also can potentially affect the dissolution rate by altering its driving force. The thermodynamic driving force for dissolution is related to the solution's saturation state relative to the solubility product of gypsum. The Gibbs-Thomson effect relates particle size to changes in the chemical potential relative to its bulk value,

$$\Delta\mu = \frac{2\gamma V_m}{r}$$

where μ is the chemical potential of a component in the solid, γ is the surface energy, V_m is the molar volume, $5.9 \times 10^{-5} \text{ m}^3 \text{ mol}^{-1}$, and r is the radius of a particle that is assumed here to be spherical. Taking the maximum reported value for the surface energy of the gypsum-water interface, $\gamma = 0.12 \text{ J m}^{-2}$ [41], yields $\Delta\mu \leq 28 \text{ J mol}^{-1}$ for a particle with diameter of 1 μm , which is close to the size of the smallest particles observed in this study. However, the standard molar Gibbs energy of gypsum dissolution is 26.1 kJ mol^{-1} , so the Gibbs-Thomson effect likely changes the solubility by no more than 0.05 % even for the smallest particles, and therefore can safely be neglected here.

The apparent activation enthalpy, ΔH^* , is constant within the examined range of solution saturations, at least to within the measurement uncertainty (see Fig. 7 and Table 2). This suggests that the rate-controlling step for gypsum dissolution is qualitatively unaffected by the thermodynamic driving force within this range of saturations. Moreover, that rate-controlling step is likely to be a surface reaction step rather than ion transport away from the surface because activation energies for ion diffusion in water are typically about half the values measured here.

Lasaga and Lüttge have suggested that for crystal dissolution, chemical bonds at kink sites are continually breaking and reforming, so the activation energy should be related to the energy required to simultaneously break all of the chemical bonds to an atom at a kink site to enable detachment from the site [42]. In gypsum, calcium ions are coordinated by eight oxygens, six of which are shared with a sulfate tetrahedral corner or another calcium ion, and two of which are part of structural water units (Fig. 8). The six “non-water” bonds are somewhat shorter and stronger than the other two. If the rate-controlling step of gypsum dissolution were to be, for example, detachment of calcium ions from kink sites, the activation energy may then be associated with the average energy to break the three calcium-oxygen ionic bonds at a calcium kink site that are not associated with water. The subsequent detachment of a calcium ion from the surface, already bonded to two water molecules, could then rapidly form a hydrated $\text{Ca}(\text{OH})_2^{2+}$ ion in solution by bonding to four more waters.

The calculated rates of gypsum dissolution depend sensitively on the measured or assumed specific surface area, as already discussed, but the activation energy is relatively insensitive to surface area. To demonstrate this, Table 2 also includes the activation enthalpy gypsum dissolution that result by alternately assuming (1) that S increases with mass loss as it would for a collection of monodisperse shrinking particles, or (2) that S remains fixed at its initial value. The activation enthalpy calculated using either of these assumptions fall in the same range, 30 kJ mol^{-1} to 40 kJ mol^{-1} , as that found by modeling the measured S changes. In addition, the activation energies reported for gypsum dissolution in earlier studies [11,18] are also in that same range, even though they used a rotating disc method in which the surface area is taken to be the geometric area of the disc face. The insensitivity of activation energy to surface area of a dissolving solid is

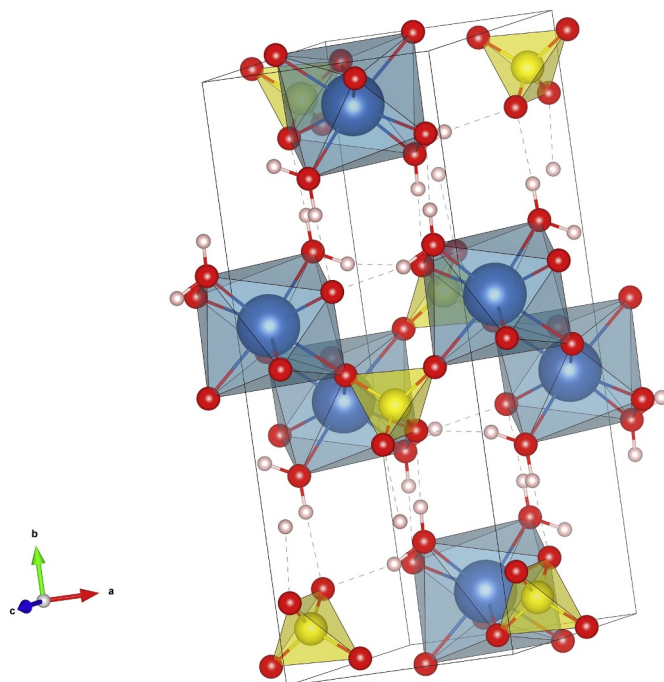


Fig. 8. The molecular structure of gypsum is obtained by VESTA 3D visualization program. The blue balls represent calcium; the yellow balls represent sulfur; the red balls represent oxygen; and the light pink ball represent hydrogen. (For interpretation of the references to color in this figure legend, the reader is referred to the web version of this article.)

consistent with the fact that the activation energy depends solely on local molecular processes such as bond breaking at kink sites.

Kinetic properties of cementitious minerals, both for dissolution and for growth, are key to understanding the evolution of the microstructure and properties of concrete binders. This is true especially at early ages, but even at longer times when mature concrete may be undergoing chemically-induced deterioration. Dissolution kinetics of gypsum, like those acquired in this study, form one small part of a larger effort that is needed to fill in the existing knowledge gaps about cement hydration and degradation. Rate constants, rate equations, and activation energies, for cement components reacting in water could form part of a valuable data repository that, together with more mature geochemical thermodynamic databases, represents a potent tool for understanding and prediction of concrete's time-dependent behavior.

5. Summary

A synthetic gypsum powder with a bimodal particle size distribution was used to examine the dependence of its dissolution rate on surface area and temperature. A decrease in specific surface area during dissolution was measured and modeled as a linear function of the dissolved mass. The observed decrease in specific surface area is likely due to the rapid annihilation of the smallest particles. The surface area measurement in this study was compared with assumptions in previous studies of uniform particle shrinkage or constant specific surface area and indicates, as expected, that such assumptions can lead to significant variations in the instantaneous rates inferred from measurements of the kind made here and in similar studies.

The surface area-normalized dissolution rate can be modeled by Eq. (2) by constraining $\alpha = 1$, as also indicated by a recent study [13]. Regression of the data to that equation yields estimates of the rate coefficient, J_0 , which increases with increasing temperature as expected. The exponent n in Eq. (2) is approximately 1.5 at all temperatures examined here. This, along with the fact that Arrhenius plots retain the same slope within that at all temperatures, suggests that the

dissolution mechanism does not change within that temperature range.

The apparent activation enthalpy, ΔH^* , is approximately 34 kJ mol^{-1} within the examined range of Q/K . This value is significantly greater than the activation energy expected if ion diffusion away from the surface were the rate-controlling step and, therefore, indicates that a surface reaction step is controlling the rate. If the activation energy is related to the energy required to break the chemical bonds at kink sites on the gypsum-water interfaces, it would help explain why other salts with octahedrally coordinated calcium exhibit a similar range of activation energies of dissolution.

CRedit authorship contribution statement

Qingxu Jin: Investigation, Methodology, Resources, Validation, Formal analysis, Project administration, Writing - original draft, Writing - review & editing. **LaKesha N. Perry:** Investigation, Methodology, Resources, Formal analysis. **Jeffrey W. Bullard:** Conceptualization, Methodology, Formal analysis, Project administration, Writing - review & editing, Supervision, Funding acquisition.

Declaration of competing interest

The authors declare that they have no known competing financial interests or personal relationships that could have appeared to influence the work reported in this paper.

Acknowledgments

Qingxu Jin gratefully acknowledges the financial support from National Science Foundation via Grant No. CMMI-1362843. Any opinions, findings, and conclusions or recommendations expressed in this material are those of the author(s) and do not necessarily reflect the views of the National Science Foundation. The authors would like to thank Paul Stutzman (NIST) for his assistance with electron microscopy.

References

- [1] T. Matschei, B. Lothenbach, F.P. Glasser, Thermodynamic properties of Portland cement hydrates in the system $\text{CaO-Al}_2\text{O}_3\text{-SiO}_2\text{-CaSO}_4\text{-CaCO}_3\text{-H}_2\text{O}$, *Cem. Concr. Res.* 37 (2007) 1379–1410.
- [2] C. Roosz, P. Vieillard, P. Blanc, S. Gaboreau, H. Gailhanou, D. Braithwaite, V. Montouillout, R. Denoyel, P. Henocq, B. Madé, Thermodynamic properties of C-S-H, C-A-S-H and M-S-H phases: results from direct measurements and predictive modelling, *J. Appl. Geochem.* 92 (2018) 140–156.
- [3] R.J. Myers, S.A. Bernal, J.L. Provis, A thermodynamic model for C-(N)-A-S-H gel: CNASH_{ss}. Derivation and validation, *Cem. Concr. Res.* 66 (2014) 27–47.
- [4] J. Haas, A. Nonat, From C-S-H to C-A-S-H: experimental study and thermodynamic modelling, *Cem. Concr. Res.* 68 (2015) 124–138.
- [5] D. Damidot, B. Lothenbach, D. Herfort, F.P. Glasser, Thermodynamics and Cement science, *Cem. Concr. Res.* 41 (2011) 679–695, <https://doi.org/10.1016/j.cemconres.2011.03.018> special Issue: 13th International Congress on the Chemistry of Cement.
- [6] P. Juilland, E. Gallucci, R.J. Flatt, K.L. Scrivener, Dissolution theory applied to the induction period in alite hydration, *Cem. Concr. Res.* 40 (6) (2010) 831–844.
- [7] W. Lerch, The influence of gypsum on the hydration and properties of Portland cement pastes, *Proceedings of the American Society for Testing and Materials*, 46 1946, pp. 1252–1291.
- [8] F.J. Tang, E.M. Gartner, Influence of sulphate source on Portland cement hydration, *Adv. Cem. Res.* 1 (2) (1988) 67–74.
- [9] P. Hewlett, M. Liska, *Lea's Chemistry of Cement and Concrete*, Butterworth-Heinemann, Oxford, United Kingdom, 2019.
- [10] A. Jeschke, K. Vosbeck, W. Dreybrodt, Surface controlled dissolution rates of gypsum in aqueous in solutions exhibit nonlinear dissolution kinetics, *Geochim. Cosmochim. Acta* 65 (2001) 27–34.
- [11] A.L. Lebedev, Kinetics of gypsum dissolution in water, *Geochem. Int.* 53 (9) (2015) 811–824.
- [12] L. Briese, R.S. Arvidson, A. Lüttge, The effect of crystal size variation on the rate of dissolution — a kinetic Monte Carlo study, *Geochim. Cosmochim. Acta* 212 (2017) 167–175, <https://doi.org/10.1016/j.gca.2017.06.010>.
- [13] J. Tang, J.W. Bullard, L.N. Perry, P. Feng, J. Liu, An empirical rate law for gypsum powder dissolution, *J. Cryst. Growth* 498 (2018) 96–105.
- [14] A.C. Lasaga, *Kinetic Theory in the Earth Sciences*, Princeton University Press, Princeton, NJ, 1998.
- [15] P.K. Mehta, P.J.M. Monteiro, *Concrete: Microstructure, Properties, and Materials*, 4th Ed., McGraw-Hill, New York, NY, 2006.
- [16] Z. Bofang, *Thermal Stresses and Temperature Control of Mass Concrete*, Butterworth-Heinemann, Oxford, United Kingdom, 2014.
- [17] A.F.M. Barton, N.M. Wilde, Dissolution rates of polycrystalline samples of 394 gypsum and orthorhombic forms of calcium sulfate by a rotating disc method, *Trans. Faraday Soc.* 67 (1971) 3590–3597.
- [18] A.L. Lebedev, A.V. Likhov, Kinetics of dissolution of natural gypsum in water at 5–25 °C, *Geochem. Int.* 6 (1989) 865–874.
- [19] D. Bosbach, W. Rammensee, In situ investigation of growth and dissolution on the (010) surface of gypsum by scanning force microscopy, *Geochim. Cosmochim. Acta* 58 (1994) 843–849.
- [20] D. Bosbach, J.L. Junta-Rosso, U. Becker, M.F. Hochella, Gypsum growth in the presence of background electrolytes studied by scanning force microscopy, *Geochim. Cosmochim. Acta* 60 (17) (1996) 3295–3304.
- [21] C. Hall, D.C. Cullen, Scanning force microscopy of gypsum dissolution and crystal growth, *AICHE J.* 42 (1996) 232–238.
- [22] H. Shindo, A. Seo, M. Itasaka, T. Odaki, K. Tanaka, Stability of surface atomic structures of ionic crystals studied by atomic force microscopy observation of various faces of CaSO_4 crystal in solution, *J. Vac. Sci. Technol.* 14 (2) (1996) 1365–1368.
- [23] C. Fan, H.H. Teng, Surface behavior of gypsum during dissolution, *Chem. Geol.* 245 (2007) 242–253.
- [24] A. Burgos-Cara, C.V. Putnis, C. Rodriguez-Navarro, E. Ruiz-Agudo, Hydration effects on gypsum dissolution revealed by in situ nanoscale atomic force microscopy observations, *Geochim. Cosmochim. Acta* 179 (2016) 110–122.
- [25] B. Zareepolgardani, A. Piednoir, J. Colombani, Gypsum dissolution rate from atomic step kinetics, *J. Phys. Chem. C* 121 (2017) 9325–9330.
- [26] A. Kumar, J. Reed, G. Sant, Vertical scanning interferometry: a new method to measure the dissolution dynamics of cementitious minerals, *J. Am. Ceram. Soc.* 96 (9) (2013) 2766–2778.
- [27] P. Feng, A.S. Brand, L. Chen, J.W. Bullard, In situ nanoscale observations of gypsum dissolution by digital holographic microscopy, *Chem. Geol.* 460 (2017) 25–36.
- [28] A. Kumar, J. Reed, G. Sant, Vertical scanning interferometry: a new method to measure the dissolution dynamics of cementitious minerals, *J. Am. Ceram. Soc.* 96 (2013) 2766–2778.
- [29] A.E. Nielsen, Electrolyte crystal growth mechanisms, *J. Cryst. Growth* 67 (1984) 289–310.
- [30] S. Glasstone, K.J. Laidler, H. Eyring, *The Theory of Rate Processes*, McGraw-Hill, New York, 1941.
- [31] L.S. Darken, R.W. Gurry, *Physical Chemistry of Metals*, McGraw-Hill, New York, 1953.
- [32] D. Kulik, S. Dmytrieva, G. Kosakowski, S. Nichenko, G. Miron, A. Leal, T. Wagner, Gibbs Energy Minimization Software for Geochemical Modeling, *Techniques and Methods*, Paul Scherrer Institut, Schweiz, 2013, <http://gems.web.psi.ch>.
- [33] B. Lothenbach, D.A. Kulik, T. Matschei, M. Balonis, L. Baquerizo, B. Dilnesa, G.D. Miron, R.J. Myers, Cemdata18: a chemical thermodynamic database for hydrated Portland cements and alkali-activated materials, *Cem. Concr. Res.* 115 (2019) 472–506.
- [34] A. Lasaga, A. Lüttge, Variation of crystal dissolution rate based on a dissolution step wave model, *Science* 291 (2001) 2400–2404.
- [35] R.S. Arvidson, I.E. Ertan, J.E. Amonette, A. Lüttge, Variation in calcite dissolution rates: a fundamental problem? *Geochim. Cosmochim. Acta* 67 (9) (2003) 1623–1634.
- [36] C. Fischer, R.S. Arvidson, A. Lüttge, How predictable are dissolution rates of crystalline material? *Geochim. Cosmochim. Acta* 98 (2012) 177–185.
- [37] C. Fischer, I. Kurganskaya, T. Schäfer, A. Lüttge, Variability of crystal surface reactivity: what do we know? *Appl. Geochem.* 43 (2014) 132–157.
- [38] C. Fischer, S. Finkeldei, F. Brandt, D. Bosbach, A. Lüttge, Direct measurement of surface dissolution rates in potential nuclear waste forms: the example of pyrochlore, *ACS Appl. Mater. Interfaces* 7 (2015) 17857–17865.
- [39] A.S. Brand, P. Feng, J.W. Bullard, Calcite dissolution rate spectra measured by in situ digital holographic microscopy, *Geochim. Cosmochim. Acta* 213 (2017) 317–329, <https://doi.org/10.1016/j.gca.2017.07.001>.
- [40] P.M. Dove, N. Han, J.J. De Yoreo, Mechanisms of classical crystal growth theory explain quartz and silicate dissolution behavior, *Proc. Natl. Acad. Sci. U. S. A.* 102 (43) (2005) 15357–15362.
- [41] A.E. Nielsen, O. Sönnel, Interfacial tensions electrolyte crystal-aqueous solution, from nucleation data, *J. Cryst. Growth* 11 (1971) 233–242.
- [42] A.C. Lasaga, A. Lüttge, Mineralogical approaches to fundamental crystal dissolution kinetics, *Am. Mineral.* 89 (4) (2004) 527–540.